Department of Physics and Astronomy
University of Heidelberg

Bachelor Thesis in Physics
submitted by

Jan Hubrich

born in Donaueschingen(Germany)

2022

Analysis of the influence from prompt $\Xi_c^{\pm}$ hadrons on the Primary Vertex in Simulated Data

This Bachelor Thesis has been carried out by Jan Hubrich at the
Physikalisches Institut, University Heidelberg
under the supervision of
Prof.Dr.Silvia Masciocchi

Abstract

High energy particle colliders are used to study the particles that make up the universe, together with their interacting forces. To accurately study particles, that decay very fast, such as heavy-flavour hadrons, the accuracy and correctness of the points of interest in high energy collisions have to be secured. The points of interest being the initial collision point and decay vertices, where certain hadrons decay.
This thesis presents analysis on the primary vertex of simulated proton-proton collisions at centre-of-mass energies of 13TeV with simulated detector response of the ALICE detector setup at LHC from Run 2. Systematic shifts of the primary vertex are examined as a function of number of tracks, used to estimate the primary vertex position. The spatial resolution of the involved tracking detectors are compared to the spatial resolution found by the residual distributions of the primary vertex. The estimated uncertainties on the initial collision point are evaluated aswell.
The introduction of $\Xi_c^{\pm}$ hadrons into simulated events and its influence on the primary vertex are compared to previous evaluation, to learn, if short lived particles can have an influence on the spatial resolution and shift of the primary vertex. The Kalman Filter particle package is used, to be able to remove reconstructed daughter tracks from the $\Xi_c^{\pm}$ hadron decay and verify the claim, that these daughter tracks are the reason the primary vertex is possibly shifted. The possible shift is then compared to the spatial resolutions aswell, to verify the correctness of the position of the primary vertex in the presence of a short lived particle such as the $\Xi_c^{\pm}$, within the uncertainties.

Zusammenfassung

Hochenergetische Teilchenkollidierer werden benutzt, um die Teilchen zu untersuchen, die das Universum ausmachen, zusammen mit ihren wecheslwirkenden Kräften. Um Teilchen, die schnell zerfallen, wie zum Beispiel Heavy-Flavour Hadronen, akkurat zu studieren, ist es wichtig, dass deren Interaktionspunkte so genau und korrekt wie möglich bestimmt werden. Wobei die wichtigen Interaktionspunkte der initiale Kollisionspunkt, sowie der Punkt, an dem bestimmte Hadronen zerfallen, sind.
In dieser Arbeit wird die Analyse von dem primären Vertex in simulierten Proton-Proton Kollisionen, bei einer Schwerpunktsenergie von 13TeV, mit den simulierten Detektorintearktionen von dem ALICE Detektoraufbau am LHC von Run 2, vorgestellt. Systematische Verschiebungen von dem primären Vertex werden untersucht als Funktion von der Anzahl an Partikelspuren, die benutzt wurden, um die Position von dem primären Vertex zu rekonstruieren. Die räumliche Auflösung der beteiligten Detektoren wird verglichen mit der räumlichen Auflösung, die durch das Residuum des primären Vertizes bestimmt wurde. Die abgeschätzten Fehler auf die initiale Position der Kollision, wird ebenfalls untersucht.
Die Einführung des $\Xi_c^{\pm}$ Hadrons in simulierte Kollisionsereignisse und dessen Einfluss auf den primären Vertex werden verglichen mit der vorherigen Untersuchung, um herauszufinden, ob das Hadron einen Einfluss auf die räumliche Auflösung und Position des primären Vertex hat. Das Kalman-Filter-Teilchenpaket wird benutzt, um die Töchterteilchen des zerfallenen $\Xi_c^{\pm}$ Hadrons aus der rekonstruktion des primären Vertizes zu entfernen und herauszufinden, ob die Behauptung stimmt, dass diese Töchterteilchen der Grund für eine mögliche Verschiebung des primären Vertizes sind. Die mögliche Verschiebung wird ebenfalls mit der räumlichen Auflösung verglichen, um zu bestätigen, dass die Position des primären Vertizes in der Anwesenheit von kurz lebigen Teilchen wie das $\Xi_c^{\pm}$, immer noch innerhalb der Unsicherheiten, korrekt ist.

Contents

1 Physics Motivation

1.1 Standard Model

In the Standard Model (SM), fundamental particles are described, together with the forces, that act on these particles (Figure 1). The particles are categorised into half-spin fermions and integer spin bosons. Fermions have three generations with increasing mass and are further divided into quarks and leptons. There are six different quarks and six different leptons, together with their respective anti-particles. Those have the same mass, but opposite charges.
Each of these particles, together with its mass, charge and spin, can be found in Figure 1. Furthermore, because quarks also interact strongly, compared to leptons, they also carry one of three color charges, red, green and blue. Similarly to electric charge, antiquarks carry the opposite color charge, called anti-color. Those anti-color charges behave in a way, such that a color and its anti-color charge cancel each other out. The three different color charges together result in a color charge neutral state also.
Quarks and leptons also come in three generations, denoted as I, II and III in Figure 1. Generations have similar properties, but different mass, increasing in each generation.
Gluons are the bosons mediating the strong force, that can exchange color charge between different quarks. Photons mediate the electro-magnetic force, and the Z and $W^{+/-}$-bosons mediate the weak force. There is no known boson yet, that corresponds to the gravitational force, therefore gravitation is not yet included in the standard model. Albeit, in most particle physics phenomena, gravitation is negligibly small compared to the other forces. The Higgs boson is the reason the other particles have mass.

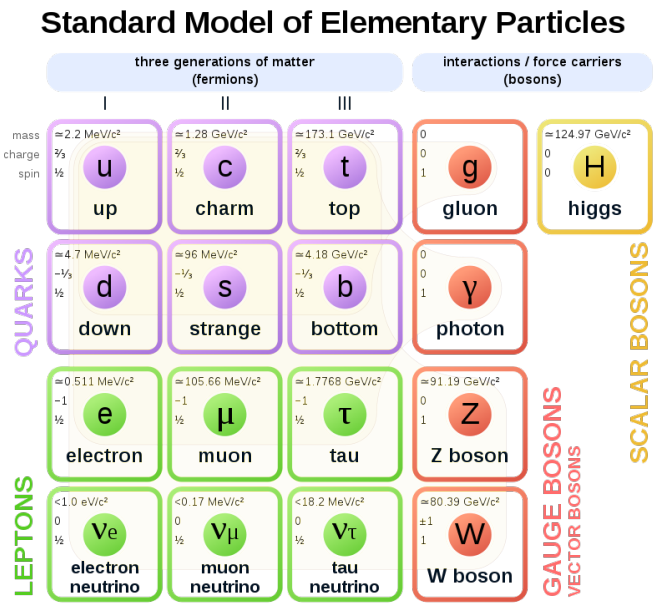

Figure 1: Elementary particles of the SM [11]

1.1.1 Strong Force

As mentioned in the previous section, the particles that interact strongly are quarks and gluons. The unique thing about the strong force can be seen in the equation of the potential between two partons, that is described as follows:

$$V(r) = -\frac{4}{3}(\hbar c)\frac{\alpha_s}{r} + kr \tag{1}$$

r is the distance between the two color charged particles, $\hbar$ is the reduced Planck constant, c is the speed of light, and k is the spring constant. α_s is the coupling constant for the strong force. Even though it is called a constant, α_s depends on the momentum transfer q^2 of the process in consideration. For high energy transfers, α_s is small enough, such that pertubative Quantum Chromo Dynamics (QCD) is calculable. This is not the case if q^2 is small. In this case α_s is approximately equal to one and pertubative QCD calculations are not aplicable.
Since Equation 1 has a linear scaling component, the potential between two quarks increases linearly with increasing distance, while the other term in this equation is tending to zero. When pulling two quarks with opposing color charge away from each other, the energy in this potential increases until creating a quark anti-quark pair, between the initial quark pair, is energetically preferable, resulting in color neutral state again.
This causes the so called color confinement of quarks, meaning single quarks cannot be observed. Only pairs of quark and anti-quark with opposite color charge, or triplets with three different color charges can be observed. The former are called mesons (quark anti-quark pair), the latter are called baryons with three different color charges. Mesons and baryons are called hadrons.

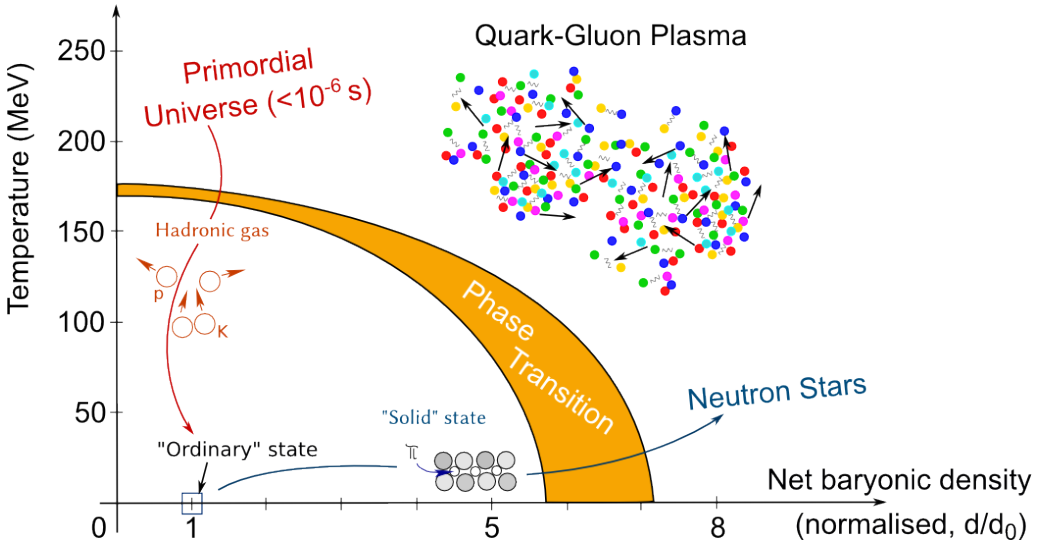

Figure 2: phase diagram of strongly-interacting matter [10]

If the energy density in a system is high enough, quarks have enough energy to move at distances larger than the typical dimension of hadrons and can become deconfined.

High energy density occurs in a system at high temperature, high baryonic density or both together as shown in Figure 2. According to Lattice QCD [4], these states can be reached by colliding ultra relativistic protons or heavy ions with each other in particle accelerators such as the Large Hadron Collider (LHC) at CERN. The resulting quark-gluon plasma (QGP) only exists for a short time of about 10 $\frac{fm}{c}$, because this system expands rapidly, until the energy density is not high enough to have deconfined quarks.

1.2 Hadronisation

When the QGP cools down sufficiently, the deconfined quarks confine back into their hadronic states. This process is called hadronisation. How this is happening cannot be directly measured, due to the very short lifetime of the QGP in high energy collisions. Only hadrons, that are produced at the freeze-out of the QGP, can be measured in a detector. This freeze-out point can be calculated with lattice QCD, to determine a temperature at which quarks are confined in hadrons again. Therefore, different theories are compared to measured data to see, which theories can most accurately describe the result. For the theories to be acknowledged, they have to be thoroughly tested under different initial conditions and with different parameters. Two of these major approaches to explain hadronisation are fragmentation and coalescence. In high energy proton-proton collisions at ultra relativistic energies at $\sqrt{s} = 13TeV$, the energy is not high enough to form a QGP. Though, how quarks hadronise in such a system can be described by the following two approaches.

1.2.1 Fragmentation

Fragmentation does not need the QGP to explain how hadrons are formed in particle collisions. It is used with a factorisation approach, in which the hadron yield is calculated, including three factors. One of those factors is the fragmentation function. The other two factors are the parton distribution function, describing the incoming partons, and the cross section relative to the hard scattering. This is calculated with known cross sections of the incoming partons, assuming high momentum transfer q^2. The fragmentation function describes the probability that an outgoing parton, produced in the hard scattering process, is part of a specific hadron [7]. These fragmentation functions, that were observed and measured in experiments, are in agreement with different collision systems at LEP and HERA [9].

1.2.2 Coalescence

Coalescence generally describes two or more particles recombining into one. This can happen at any scale, but in the case of hadronisation, the focus lies on quarks. If two or more quarks are close to each other in phase-space, they can recombine to form a color neutral hadron again, after being deconfined in the QGP. This approach needs knowledge of how quarks are distributed in phase-space in the QGP, to make predictions on different hadrons yields. This makes it hard to generalise yields in different collision systems, since those can be very different from each other, and needs more knowledge of the evolution of the QGP to make accurate predictions.

1.3 Heavy-flavour hadrons and the Ξ_c^+ baryon

Heavy-flavour hadrons are particles, that contain at least one of the heavier quarks, namely charm or bottom. Among those is the Ξ_c^+ baryon, which impact is analised in this thesis. The Ξ_c^+, toghether with its charged conjugated antiparticle (Ξ_c^-), is a particle consisting of an up, a strange and a charm quark (anti-up, anti-strange, anti-charm quark in the case of Ξ_c^-) [2]. These heavy flavour particles are of interest to verify the theories of hadronisation. Since it was found that some theories of hadronisation, that were confirmed in e^+e^-, were not universal, if heavier ions and higher energies were used in collisions. Especially when heavy flavour particles were taken in cosideration. Thus, heavy flavour particles have to be investigated to compare the production of those to the different theories and simulated models. This was already done for Λ_c, Ξ_c^0 and Ω_c^0. These heavy flavour particles together with the Ξ_c^+ have a very short lifetime of 60 to 500 $\cdot 10^{-15}$s [12]. This means, that those particles cannot be measured directly. Instead, they have to be measured by reconstructing their decay chain and an invariant mass analysis.

1.3.1 Reconstruction of short lived Heavy Flavour particles

The reconstruction of short lived heavy flavour particles comes with some problems. Not all decay channels of the particles are perfectly known. Therefore, most of the time, only one branch of all decay channels is measured. Together with the branching ratio, that is known from calculations, the whole number of original candidates can be calculated.
Secondly, the daughter particles are often particles, that are also formed in other decays. This results in a high background of particles, which need to be filtered out. This filtering process is done by calculating the invariant mass of candidate daughter particles. If the calculated invariant mass is similar to the mass of the mother particle, those potential daughter particles are considered to be from the searched mother particle. Since there are many potential daughter candidates, this results in a high combinatorial background, and therefore this step of the analysis needs a lot of computing power.

$$m_{mother}c^2 = \sum_{i=0}^{n} \boldsymbol{p_i} \tag{2}$$

$\boldsymbol{p_i}$ are the 4-vectors of the n daughter particles, which decayed from the mother.

Depending on the decay itself, there are other variables that can be utilised to filter out wrong potential candidates, or to increase the efficiency of the whole process. Since there are a lot of particles created in high energy collisions, it is not feasible to filter out every wrong candidate with good efficency. Instead, the number of candidates is approximated with a fit on the mass peak. For that, a good signal to background ratio (right to wrong candidates ratio) suffices. To extract the number of all mother particles created in a collision, the mass peak is integrated and from that, an approximation of found mother particles can be made. After that, the efficiency of all filtering methods that were used is calculated with simulated data.

1.3.2 Ξ_c^+ decay channel

One decay channel of the Ξ_c^+ particle is

$$\Xi_c^+ \to \Xi^- \pi^+ \pi^+ \tag{3}$$

,where Ξ^- decays further as follows

$$\Xi^- \to \Lambda^0 \pi^- \tag{4}$$

$$\Lambda^0 \to p\pi^- \tag{5}$$

This decay has a branching ratio of $(2.9 \pm 1.3)\%$ according to [2]. The whole decay chain is the same for the anti-particle Ξ_c^-, where the daughters are also charge conjugated. The topology of this whole decay process is visualised in Figure 3.

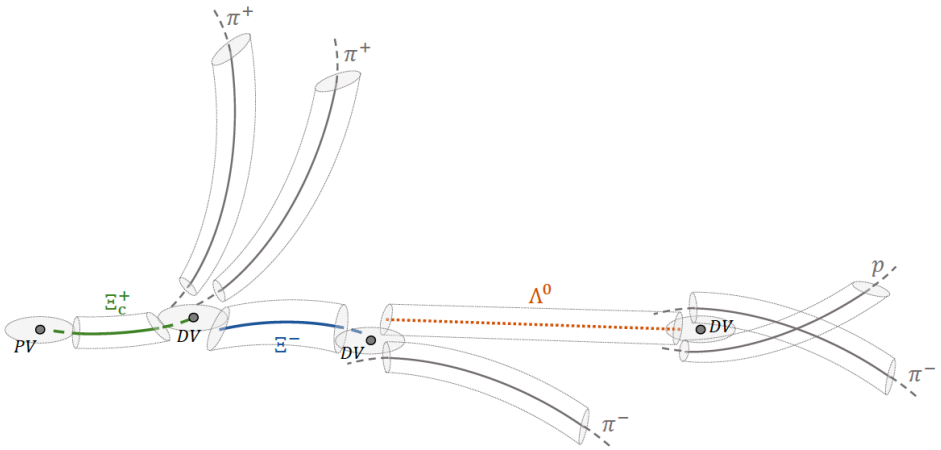

Figure 3: Decay topology of Equation 3 [14]

The Primary Vertex (PV), on the left in Figure 3, is the origin of this decay. The rings and tubes around the vertices and tracks visualise their uncertainties. This topology implies the presence of a magnetic field. The magnetic field causes a force on moving charged particles, namely the Lorentz force, forcing them onto curved tracks. By knowing the identity of a particle, together with the radius of its curvature in a known magnetic field, their initial 4-vector at their starting vertex can be calclulated. With Equation 2, this procedure is able to determine the invariant mass of the initial particle Ξ_c^+, only from the outgoing $\pi^\pm$ and proton (p) in Figure 3.

1.4 Analysis Motivation

Measured yields of heavy flavour baryons, such as Λ_c and Ξ_c^0, compared to heavy flavour mesons (D^0) in proton-proton collisions with a centre-of-mass energy of $\sqrt{s} = 13TeV$, are not in agreement with the latest hadronisation models, including fragmentation and coalescence [18], as shown in Figure 4. Especially in low p_T (transverse[1] momentum) regions, the theoretical models and the measured data differ by a factor of over two.

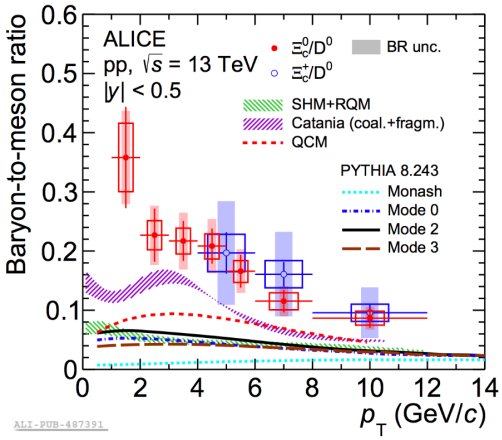

Figure 4: baryon-to-meson yield ratio with p_T dependence, together with theoretical models, describing the same collision system[18]

This incentivises better measurements for heavy flavour particles, particulary in the low transverse momentum range ($p_T \leq 1GeV$). Good measurements of particle collisions require a good understanding of the original collision point and its parameters. This raises the question, if heavy flavour particles, such as the Ξ_c^+, have an impact on the accuracy of the PV. After all, in the low p_T range, there is a big combinatorial background of candidates, that makes it hard to find an accurate yield of those heavy flavour particles. Hence, it is important to seperate the primary and secondary vertex, to differenciate between daughter particles of a heavy flavour decay and similar particles that also come from the PV.

This thesis focuses on the PV, the initial collision point, of a proton-proton collision in simulated data, modelled after the ALICE detector at CERN and previously captured data with this detector, and if there is an impact on the PV accuracy, due to the fast decay of Ξ_c^+ particles.

[1] perpendicular to the direction of the collsion beams

2 The ALICE Detector

The ALICE (A Large Ion Collider Experiment) detector is located at CERN near Geneva, 60 meters under the ground and has dimensions of 16x16x26m^3 with a total weight of 10000t [6]. It is one of four major experiments at the LHC. The LHC is capable to accelerate protons up to 6.8TeV to collide them at certain interaction points, resulting in center-of-mass energies of up to 13.6TeV. One of those interaction points being located at the center of the ALICE detector. The detector system consists of different detectors with different purposes, to reconstruct high multiplicity events with high momentum resolution and excellent particle identification [6].

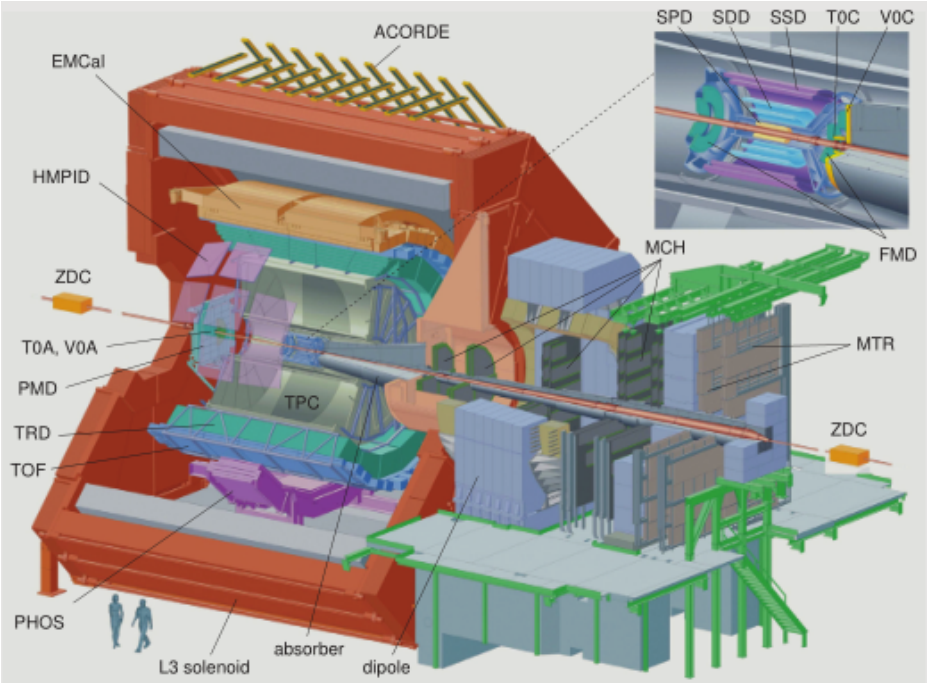

Figure 5: schematic of ALICE detectors taken from [13]

The L3 solenoid induces a magnetic field of 0.5T. The magnetic field points in the same direction as the beam pipe, that goes straight through the detector, so that charged particles travelling in the same direction as the beam pipe are not affected by the magnetic field. All detectors that make up the central barrel are inside the enclosing L3 solenoid. The detectors that are most important in the case of PV reconstruction, (the initial collision point) are the Inner Tracking System (ITS) and the Time Projection Chamber (TPC). Both of those tracking detectors rely on the particle having electric charge and therefore, only charged particle tracks are directly reconstructed in these detectors.
Aside from the two main tracking detectors, there are a lot of other detectors that are out of scope of this thesis, since they are only indirectly included in the PV reconstruction.

2.1 Coordinate System

The coordinate system in ALICE can be described as a Cartesian coordinate system with its origin in the center of the detector (top right frame of Figure 5). The z-axis is in the direction of the beampipe, the y-axis points upwards and the x-axis points towards the center of the LHC. These three axes form a right-handed Cartesian coordinate system. The x-y plane therefore also describes the transverse plane, since it is perpendicular to the z-axis. The detector systems generally offer a higher spatial resolution in this transverse plane in order to optimally reconstruct the particle trajectory, and therefore determine the particle transverse momentum as precisely as possible.
The cylindrical symmetry around the z-axis also suggests a description of the coordinate system in terms of the angles. The angle in the x-y-plane is called the azimuth angle ϕ, whereas the angle in the y-z-plane is called θ. The particals colliding do not collide central most of the time, which results in the outgoing particles created from the high energy collision to be Lorentz boosted along the z-axis. Therefore, the angle θ is not Lorentz-invariant and another quantity has to be used, that is Lorentz-invariant. This quantity is called rapidity and is defined as follows

$$y = \frac{1}{2} \ln \frac{E + p_z c}{E - p_z c} \tag{6}$$

, where y is the rapidity, E the energy of a given particle and p_z the momentum of this particle along the z-axis. If the particle is relativistic, which particles created in the collision are, the rapidity can be approximated with the pseudo-rapidity.

$$\eta = -\ln \tan \frac{\theta}{2} \tag{7}$$

To finish the description of the coordinate system with angles, the radius r is needed to fully describe the whole three dimensional space.

2.2 Inner Tracking System

The ITS is the first detector, that particles can reach, after the initial collision, and is wrapped around the beam pipe. It has a particle acceptance from -0.9 to 0.9 η as a whole, with the first layer having an acceptance of $|\eta| < 1.98$ [6]. The ITS consists of six layers that can be divided into three different groups. The first group, the two inner most layers of the ITS are located at a radius of 3.9cm and 7.6cm respectivly. Those innermost detector layers are Silicon Pixel Detectors (SPD), because of the high amount of particles that are predicted to pass this layer in heavy-ion collisions. SPD have a good enough resolution to support as many as 50 particles per cm^2 [6]. The next two layers of the ITS are Silicon Drift Detectors (SDD) at a radius of 14cm and 24cm. The last two layers of the detector are Silicon Strip Detectors (SSD) at a distance to the beam pipe of 38cm and 43cm. All three groups of the ITS consist of the semiconducter silicon, which has the advantage of a small material budget. This is especially important, so that the outgoing particles, created in the initial collision, are influenced as little as possible by the detector material. The outer four silicon detectors can also be used for particle identification of low momentum particles, because of their analog readout.
The ITS currently inside the ALICE detector has been recently upgraded and has different properties. The data sets discussed in this thesis were taken with the older ITS detector.

2.3 Time Projection Chamber

The TPC detector is the biggest singular detector in this whole detector arrangement. Its inner radius is 60.7cm and extends to an outer radius of 278cm around the beam pipe. Its particle acceptance is the same as the acceptance of the ITS; -0.9 to 0.9 η and covering the whole azimuth angle. It has a volume of $90m^3$ and is filled with a gas mix of neon (or argon), CO_2 and N_2. This gas is ionised by incoming charged particles. The now unbound electrons, coming from the ionised gas, are travelling along the z-axis, due to an electric field in the chamber, to the readout chambers at the endcaps of the cylinder, while the ionised gas atoms are travelling to the central electrode. The analog signal of the electrons is detected in the readout chambers. By knowing the time it takes for the electrons to reach the readout chamber the three dimensional point inside the TPC can be calculated, where the gas was initially ionised. For this to be accurate, it is important that the drift velocity of the electrons is as constant as possible in the electric field inside the TPC. According to [6], the gas mixure is optimised to provide a drift speed with low diffusion and space-charge effect, while also having a low radiation length. With this characteristics of the gas, together with the readout chambers, a track resolution of $\approx 200\mu$m can be achieved [8].
The electrons drift time makes this detector one of the slowest tracking detectors, but in return has high granularity. Still, the TPC is fast enough for the interaction rate of the particle beams in the LHC [6], The readout chambers are segmented into 159 pads. This allows a single track to have a maxium of 159 tracked points inside the TPC.

2.4 Particle Identification

While some particles such as electrons and muons are measured differently in other detectors of ALICE, the particles resulting from the Ξ_c^+ decay are identified in the TPC. As already mentioned in the ITS paragraph, the four outer layers of the ITS can be used for particle identification of low momentum particles. This can be achieved, because the analog signals of these detectors are proportional to the energy deposition of the charged particles, that cross the detector layers. Different particles have different amounts of energy that they loose to the detector material. With this energy loss different particle can be distinguished Figure 6.
This is also the case in the TPC, in which also high momentum particles can be identified, due to the specific energy loss of charged particles in the gas of the TPC. One quantity for a particle identification that is missing is its momentum. The momentum of a particle can be retrieved by the track curvature in the magnetic field of the TPC.

With those two variables, particles can be compared with the expected specific energy loss of a certain particle, that can be calculated via the Bethe equation [17]

$$\left\langle \frac{dE}{dx} \right\rangle = Kz^2 \frac{Z}{A} \frac{1}{\beta^2} \left[\frac{1}{2} \ln \frac{2m_e c^2 \beta^2 \gamma^2 W_{\max}}{I^2} - \beta^2 - \frac{\delta(\beta\gamma)}{2} \right] \tag{8}$$

$\left\langle \frac{dE}{dx} \right\rangle$: mean specific energy loss of a particle
β : relativistic speed
z : charge of particle
m_e : electron mass
c : speed of light
γ : time dilation factor
$\delta(\beta\gamma)$: correction factor
W : energy transfer of particle to electron in medium

The other variables are describing the medium that the particle loses its energy to.

The specific energy loss that is measured can then be compared to calculated specific energy loss in the followig way:

$$n = \frac{\frac{dE}{dx}_{\text{measured}} - \left\langle \frac{dE}{dx} \right\rangle}{\sigma} \tag{9}$$

$\left\langle \frac{dE}{dx} \right\rangle$ is different for each particle type

where σ is the resolution of $\frac{dE}{dx}_{\text{measured}}$ with a mass hypothesis of certain particle. $\left\langle \frac{dE}{dx} \right\rangle$ is the calculated mean specific energy loss assuming the mass of the particle in question. Measured specific energy losses that are within $|n| < 3\sigma$ using Equation 9, are considered to have been identified correctly. This can differentiate particles in a lot of momentum intervals, but in some momentum ranges there are overlaps (as seen in Figure 6) , so that a measured point cannot be assigned to one single particle. In this case the Time of Flight (TOF) detector can be used to resolve this ambiguity.
The TOF detector measures the time, when a particle crosses its detector layers. Different particles with the same specific energy loss, the same momentum, but different mass, propagate at different velocities, which results in different arrival times at the TOF. The cases where particle identification via Equation 8 do not give a definitive answer, can be answered through the difference in time of flight.

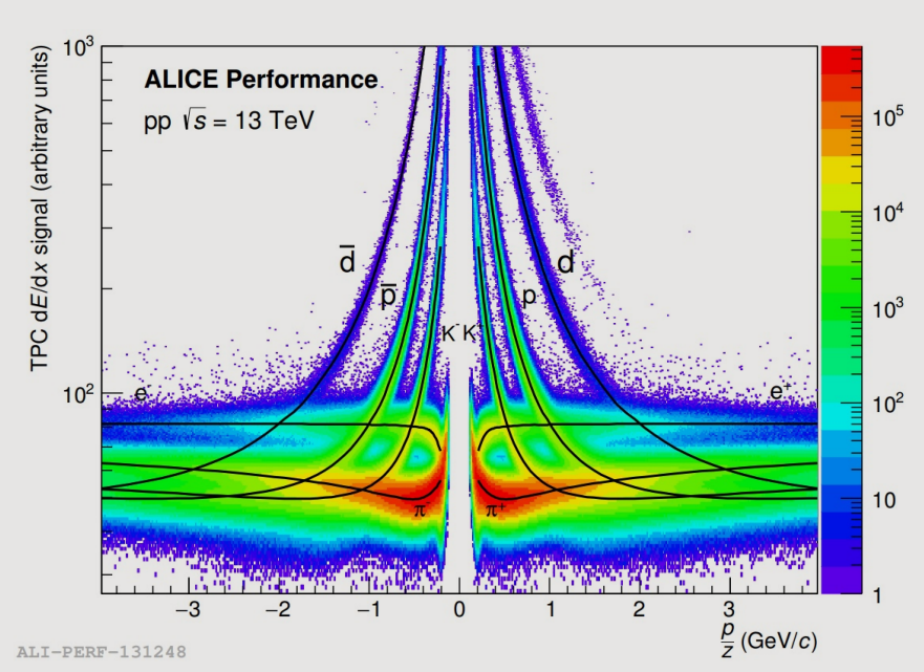

Figure 6: measured specific energy loss of different particles (colored points) compared to the expected specific energy loss (black lines) according to Equation 8, dependent on the momentum over charge. This way, particles and anti particles are separated aswell. The expected particles are denoted next to each particle band. The scale on the right depicts, how many partilces are in a certain momentum over z and specific energy loss bin.

2.5 Simulation of Data

Simulating physical processes and systems can help to understand a process or system better, and can verify the theories, that are used to make the simulations, by comparing the simulated outcomes with experimental data. The latter was done in Figure 4, where different simulation models (SHM+RQM, Catania, QCM, PYTHIA) are compared to the experimental measured bayron-to-meson yield ratios. In this case it is clear, that the simulation cannot fully describe what is happening. After such findings, simulations can be modified and improved, and theories, that may correct for the disparity, can be implemented. If a simulation is fully describing what is measured experimentally, the simulation is considered to be correct. This does not mean that the underlying theories in the simulations have to be true, since one experimental measurement is not describing what generally happens in the universe. Therefore, there has to be many iterations, to have a good physical description and understanding of hadronisation in high energy collsions, also how the detector interacts with the incoming particles.

In this thesis, two different simulated data sets are looked at (subsubsection 2.5.1, subsubsection 2.5.2, that were simulated using PHYTIA [16] as particle generator, together with GEANT [5]. PYTHIA is able to generate events of high-energy collisions. GEANT is used to simulated the expected detector responce of ALICE, together with the particle interactions with the detector material, so that the reconstruction of the particle trajectories is the same as it is measured in the experiment. The advantage here is, that the true states of the particles are known, and can be compared with the detector response and reconstruction.

Even though, the hadronisation process cannot be fully described with todays theories, the part after the hadronisation can be described pretty accurately by PYTHIA. This means, that although the general event properties, such as the true point of collision or decay vertex positions of known particles, are repoduced properly for the goal of the current study, the hadron yields are not accurate (as shown in Figure 4). After the collision, outgoing short lived particles decay, and the daughter particles, together with other particles from the initial collision, would reach the detectors. There, GEANT simulates how a particle interacts with the detector material and simulates the expected detector signal. There are a lot of different effects between detector material and incoming particles, such as ionisation, pair production, annhilation and other effects [5]. Also spallation can happen, where high energy particles unhinge particles inside detectors and structure material. For the conclusion of this thesis, both of those simulations have to be accurate. Since both simulation codes are used often regarding A Large Ion Collider Experiment (ALICE) experiments, this is assumed to be true.

2.5.1 Minimum Bias

To have even better comparability with experimental data, the simulated data used in this thesis is modelled after the Run 2 ALICE setup. The minimum bias data tries to replicate the experimental data as closely as possible.
In this case the simulated data is modelled after proton-proton collisions at centre-of-mass energies of $\sqrt{s} = 13TeV$. In proton-proton collisions the abundance of charm quarks is low. There are over 46.4 million events in the minimum bias (minbias) simulated data set, where one event refers to two protons colliding with each other. This means, that there are over 46.4 million values describing each parameter in an event, stored in a so called ROOT tree. ROOT being the analysis software to combine different variables into histograms and graph plots. One example of such a distribution from minbias data is the following true x-position of the initial collision point.

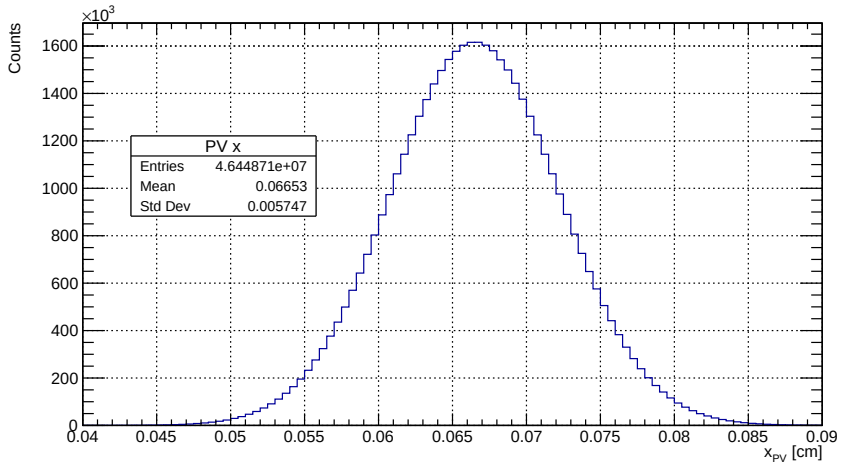

Figure 7: PV x-position in relation to the origin point in the ALICE detector

2.5.2 Introduction of Heavy Flavour particles into Simulation

The second data set for this thesis is similar to the minbias data, though it is enhanced with $\Xi_c^{\pm}$ particles. Now in every event an additional charm anti-charm pair is introduced in the simulation. The quark anti-quark pair is forced in the simulation to end up as an Ξ_c^+ or Ξ_c^- respectivley by hadronising with other quarks created in the simulated collision, or by decaying from other hadrons. The former particles, coming from the initial collision vertex are also called prompt $\Xi_c^{\pm}$, where as the latter are non-prompt, due to not coming from the PV.
The number of events in this data set is $\approx$ 25.2 million. The later analysis is focusing on the effect of $\Xi_c^{\pm}$ on the PV, meaning the non-prompt $\Xi_c^{\pm}$ are discarded in this data set. This can be easily done, because in the simulation it is known which particles are prompt or non-prompt. This brings the number of events down to 234409, which is only 0.93% of the original event count.
Because this data set introduces new particles into the collision system, the number of particles created in this simulated collision is higher compared to the minbias data set. Each singular event has at least one additional particle ($\Xi_c^{\pm}$) in it due to the artificially added charm anti-charm quarks. Since there is a $\Xi_c^{\pm}$ in each event, related values to the heavy flavour particle are also stored, such as the reconstructed transverse momentum, the reconstructed mass of $\Xi_c^{\pm}$ and its reconstructed decay length. Likewise, the true values of these quantities are also stored in the data set, aswell as the true point in space, where the $\Xi_c^{\pm}$ decayed. This vertex is also called secondary vertex. There the particle decayes into daughter particles like displayed in Figure 3.

3 Properties of the Primary Vertex

The PV represents the point where the beam particles have collided to give origin to an event of interest. The PV is reconstructed using the trajectories of the primary particles produced in the collision. The number of tracks, which are eventually used to reconstruct a given PV, is called Number of Contributors (NCont). This is a subset of all tracks belonging to one event, since there are also tracks which emerge not from the primary collision, but from secondary decays. In the case of minimum bias events the distribution of NCont looks like the following.

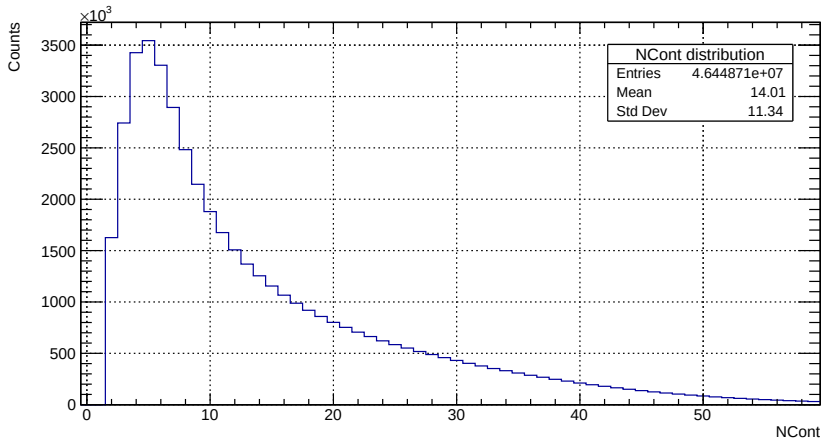

Figure 8: Distribution of the number of tracks (NCont), that were used to reconstruct the PV in simulated minbias events

At least two primary tracks are needed to reconstruct the PV, because there is no crossing point between only one track. The distribution (Figure 8) peaks at five contributors. The mean is at 14.01 contributors. The number of events with more than 50 contributors is very low.

3.1 Primary Vertex Residuals - the mean

To be able to tell how well a PV can be reconstructed, simulated data is used. In simulated data, one can obtain the true position of the PV as well as the reconstructed position. The latter is the one that is obtained in real life measurements. By having these two values, the deviation of the reconstructed compared to the true value can be calculated as follows:

$$X_{\text{PV, residual}} = X_{\text{PV, true}} - X_{\text{PV, rec}} \tag{10}$$

$X_{\text{PV, true}}$: true x-value of the PV
$X_{\text{PV, rec}}$: reconstructed x-value of the PV
$X_{\text{PV, residual}}$: difference of reconstructed and the true value of the x position

This equation is also true for the Y and Z coordinates.

Taking many events into account, these values form a distribution of the residuals. If the true position of the PV could be reconstructed perfectly, this distribution would just be a δ-function at zero. This is not the case in the real world. The detectors have systematic and statistical uncertainties, leading a finite width distribution. The way the PV is reconstructed has an influence on this distribution, as not all reconstruction algorithms yield the same performance.
A residual distribution is considered good, if the mean of the distribution is consistent with zero, and the width is as small as possible, compatible with the detector resolution. If the mean would be shifted in one direction, this would indicate a systematic error. The width of the distribution reflects the spatial resolution with which the vertex can be determined. The best possible resolution is crucial, for studying short-living particles, such as heavy-flavour hadrons.

This makes the residual a great distribution to look into and assess the quality of the PV reconstruction An example for this is the following:

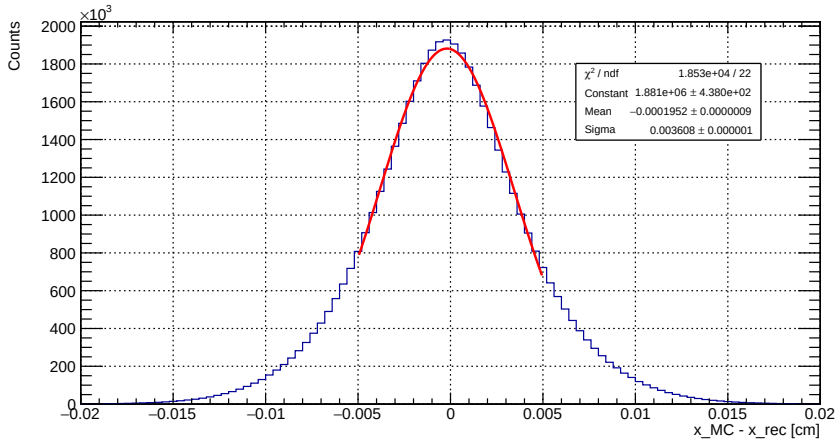

Figure 9: Residual distribution of the PV x-axis in simulated minbias data (blue), fitted with a Gaussian (red). The fit parameters are stated in the box

The residual distribution, shown in Figure 9, exhibits a typical gaussian form. The slight tension with a single gaussian fit most likely stems from the many statistical errors that occur in reconstruction, resulting in a number of convoluted gaussians. The

distribution is symmetric and extends up to maximal deviations of about 0.01cm. The mean of the distribution deviates from zero by -1.95μm, which is a non-significant shift, compared to the typical spatial resolutions of the detectors.

These residuals can be as function of the number of contributors with the assumption that higher NCont lead to better resolutions. The resulting residual then shows how well the PV can be reconstructed if that amount of tracks were used to reconstruct its position. This was done for two to 49 NCont and each of those residuals was fitted with a gaus function. The fit parameters of the fitted function are stated below (Figure 10, Figure 11).

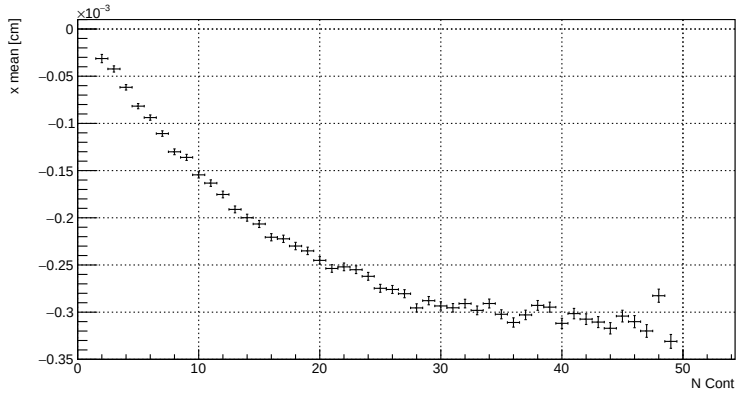

Figure 10: mean of gaus fitted residual distributions as a function of the number of contributors in simulated minbias data

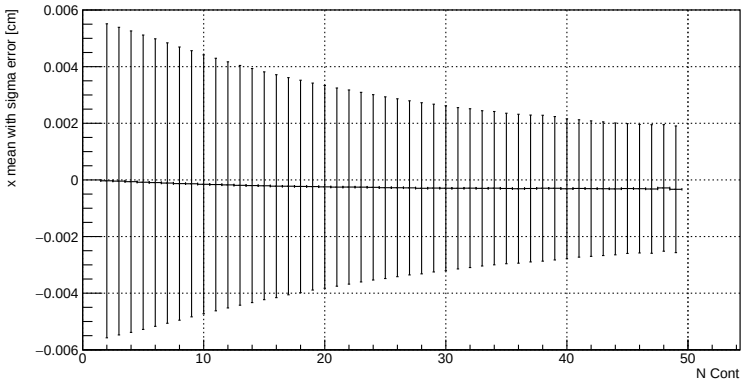

Figure 11: mean with width (1-σ) as uncertainty of gaus fitted residual distributions as a function of the number of contributors in simulated minbias data

Figure 10 shows, that for lower NCont, there seems to be a smaller shift in the mean position in x direction. This mean grows almost linearly with NCont up to 30 contributors and a value of -3 μm. In Figure 11 for low NCont the width is the highest at about 55μm. Considering the statistical uncertainties, the shift from the true position of the PV seems significant. However in Figure 11, the shift of the mean is within the width of the residual distribution, which represents the resolution. This shows that the shift is not significant. With increasing NCont the width of the residual decreases down to 20μm; increasing accuracy with higher NCont as expected.

3.2 Primary Vertex Residuals - the width

The spatial resolution on the determination of the position of the primary vertex is studied by considereing the width of the residual distribution, fitted by a gaus function. In particular, the dependence of the width in the three coordinates (x, y, z) on the number of tracks used to determine the PV is considered.

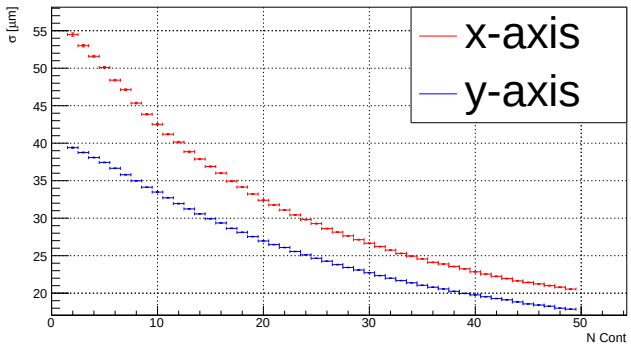

Figure 12: width of gaus fitted residual distributions in x and y as function of NCont in minbias data

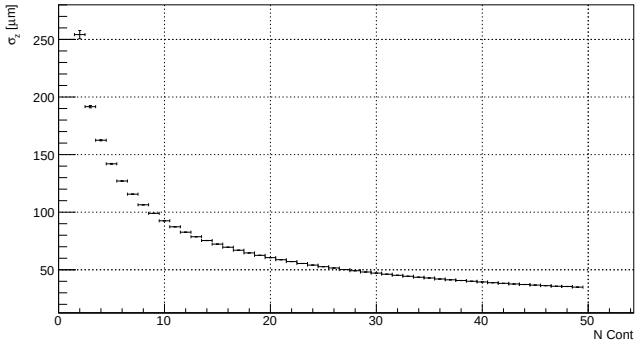

Figure 13: width of gaus fitted residual distributions in z as a function of NCont in minbias data

In Figure 12 and Figure 13, it is clearly visible, that with higher NCont the width in each direction gets smaller. This dependency of NCont is expected, because with more reconstructed tracks coming from an initial interaction point, algorithms can find the PV more accuratly.

It can be noted that the resolution on the PV z position (Figure 13) is poorer than in the x and y directions. This is explained by the asymmetric granularity of the detectors, and therefore, spatial resolution of the tracks. The tracking detectors in ALICE in Run 1 and 2 have a higher resolution in the plane transversal to the beam direction and to the magnetic field to achieve an optimal measurement of the transverse momentum. Both the ITS and the TPC detectors have poorer resolution in z compared to the x-y-plane [3] [6].
With higher NCont, the PV residual distribution widths are of the same order as the resolution of the ITS detectors ($\approx 100\mu m$ in z, $\approx 30\mu m$ in x and y). This reinforces the claim, that there is no systematic shift on the PV, while also explaining the width of the residual distribution.

3.3 Primary Vertex Residuals - the pulls

It is crucial to know for proper vertex and decay analysis, if the reconstructed uncertainties of the PV are correctly estimated, on the base of the track uncertainties and the fitting algorithm. This is done by looking into a quantity related to the residual, namely the pull. The pull is defined as follows:

$$X_{\text{PV, pull}} = \frac{X_{\text{PV, true}} - X_{\text{PV, rec}}}{\sigma_{\text{X, PV, rec}}} \tag{11}$$

$X_{\text{PV, true}}$: true x-value of the PV
$X_{\text{PV, rec}}$: reconstructed x-value of the PV
$X_{\text{PV, pull}}$: difference of reconstructed x-value compared to the true value
$\sigma_{\text{X, PV, rec}}$: reconstructed error on the x-value of the PV

This equation is also true for the Y and Z coordinates

When the uncertainty on the PV is correctly assigned, the resulting distribution of pulls should be a gaussian with a width of one. If the width of the distribution is lower than one, the uncertainty on the value could have been chosen to be too small. If it is larger than one, then the error associated with its value is underestimated. The pull is considered good, if the mean is at zero and the width is reasonably consistent with one.

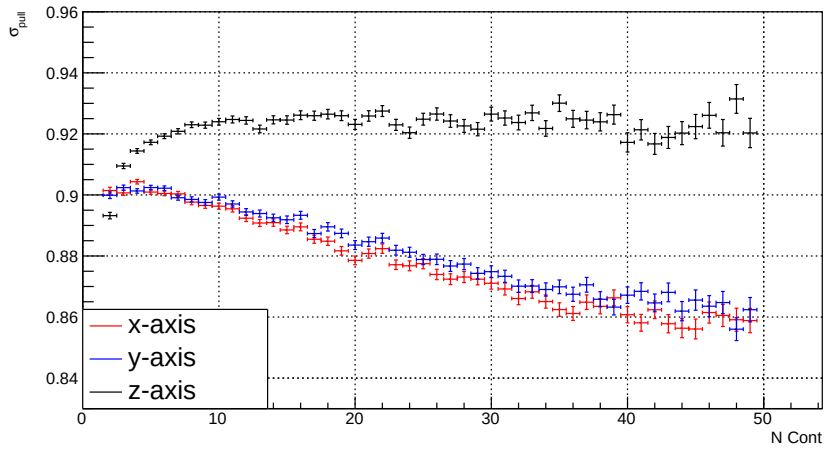

Figure 14: width of the gaus fit on the PV pull distribution as a function of NCont in minbias data

The pull width on the x- and y-axis is getting smaller with higher NCont, meaning the estimated uncertainty is not perfectly accounting for the higher precision with higher NCont. Still, all pull widths are in the range of 0.84 and 0.94 and therefore show, that the reconstructed uncertainties are of good quality and are rather too big instead of being underestimated.

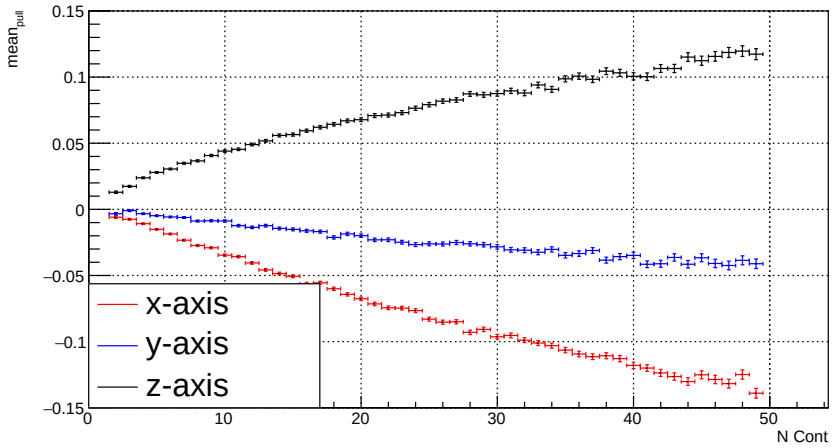

Figure 15: mean of the gaus fit on the PV pull distribution as a function of NCont in minbias data

The mean of the PV pull distribution has the same tendencies as the PV residual distribution as a function of NCont, since they are closley related. This means that the systematic shift of the PV is not accounted by the estimated uncertanties for higher NCont. As it was already argued before, that this shift is within the spatial resolution of the tracking detectors, this shift in the mean of the pull distribution can be disregarded. However, this systematic shift could get problematic, if the detector resolution is getting better. Though, a better detector resolution also could get rid of this shift, if the shift was due to previous detectors inaccuracy.

3.4 Ξ_c^+ influence on the Primary Vertex

In the primary collision many particles are formed. Some of those do not have a long enough lifetime to reach the ITS. One of those particles is the Ξ_c^+, which has an average decay length of $(c\tau)_{\Xi_c^+} = 137\mu m$. Since it does not reach any detectors, this particle can only be reconstructed via the particles it decays into. One of those decays is illustrated in Figure 3. The addional secondary particle tracks, coming from the secondary vertex may get misinterpreted to come from the PV. This may cause a shift of the PV in the direction of the secondary vertex, due to the wrongly assigned tracks contributing to the PV reconstruction.

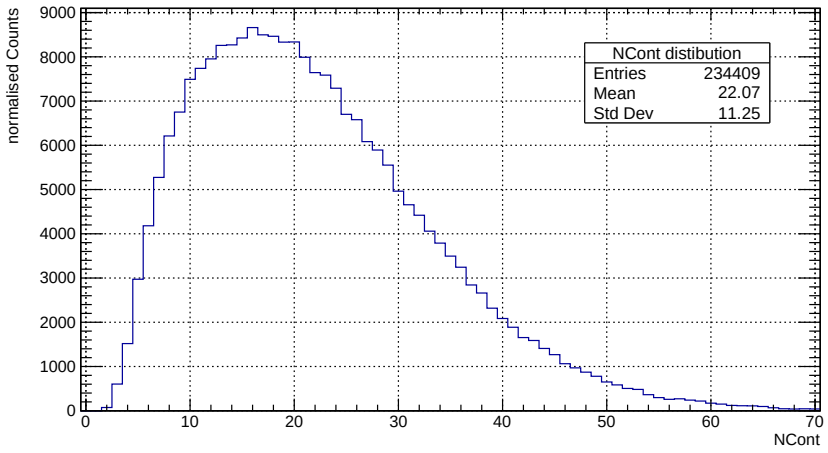

Figure 16: Distribution of NCont that were used to reconstruct the PV in simulated $\Xi_c^\pm$ enhanced data

Figure 16 depicts the same as Figure 8, but now with $\Xi_c^\pm$ enhanced events. Comparing those two histograms, it is clear, that the $\Xi_c^\pm$ enhanced NCont distribution has a higher mean of NCont aswell as a broader peak. This could be explained by the artificially injected charm quark, that results in a higher multiplicity as already mentioned in subsubsection 2.5.2.
Since the two NCont distribution in minbias data and $\Xi_c^\pm$ enhanced data are so different, instead of having a value for each single NCont, intervals are used. This is also benefits statistics, considering the $\Xi_c^\pm$ enhance data only has 234409 events with prompt $\Xi_c^\pm$.

3.4.1 Kalman Filter particle package

The Kalman Filter (KF) particle package is essential to reconstruct secondary vertices of fast decaying particles such as the $\Xi_c^\pm$, that are not detected by detectors. The KF method includes complicated math [15], and assigns every detected particle a state vector. This state vector includes position and momentum in cardinal coordinates, the energy and the type of a particle. As the position, momentum and energy of a particle changes, its state vector has to change aswell according to the measurements. This is done by iterating over the different measurements, while also accounting for errors in each iteration step. In the end, the optimum estimation of the particle track is calculated by the different state vectors previously obtained.
With the newly obtained tracks, state vectors for a decay point of mother particles can be constructed, together with a track for the mother particle aswell. For this to work, the daughter particle tracks have to be extrapolated to the position of a possible decay point. At this point the invariant mass of the mother can be calculated with the state vectors of the daughters. With the invariant mass and the participating daughter particle types, the mother particle type can be reconstructed. Decays, like in Figure 3, are even more complicated to reconstruct, due to having more than one decay vertex. In this case, this previously described step has to be done multiple times.
Since this process can extrapolate the particle tracks to their estimated initial vertex the KF can also be used to detect some non-charged particles within a decay chain. This process is also done on the simulated $\Xi_c^\pm$ enhanced data to obtain its reconstructed decay vertex.

3.4.2 Primary Vertex residual and pull distribution

Comparing the PV residual distributions in minbias data versus the $\Xi_c^\pm$ enhanced data can show, if the presence of a $\Xi_c^\pm$ has an impact on the PV. Because the event count in the case of $\Xi_c^\pm$ enhanced data is low, and because of the before mentioned reason regarding the NCont, NCont intervals are used.
In the $\Xi_c^\pm$ enhanced data, the decay daughters (especially the two pions) coming from the $\Xi_c^\pm$ decay vertex, could be falsely used for the reconstruction of the PV, resulting in the PV being shifted towards the secondary vertex. Since the secondary vertices are thought to be quasi uniformly distributed in pseudo-rapidity, the mean of the residual distribution should not change, but the width of it should increase. The assumption for this distribution is, that at high NCont the residuals are almost the same, where as at low NCont the difference between the width of residual distributions is higher.

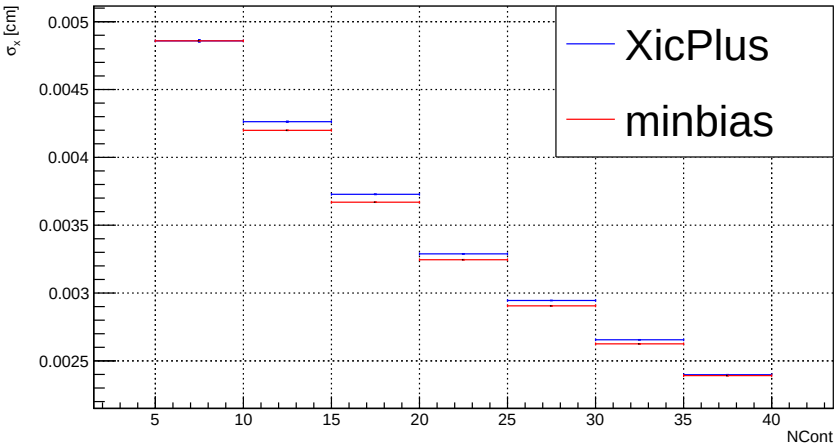

Figure 17: Comparison between the width of gaus fitted residual distributions in minbias and $\Xi_c^{\pm}$ data as a function of NCont

Eventhough the residual distribution width in $\Xi_c^{\pm}$ enhanced events is always larger in Figure 17, compared to the same value in minbias, it is not the same as the assumption. At low NCont the values are very close, where as the prediction is, that in this case, the two widths should deviate the most. Looking at all NCont intervals, the difference in residual distribution width is small compared to the difference dependent on NCont.

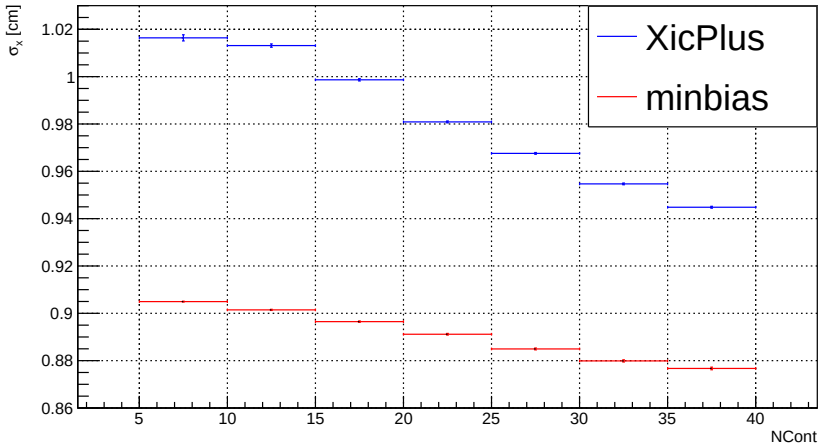

Figure 18: Comparison between the width of gaus fitted pull distributions in minbias and $\Xi_c^{\pm}$ data as a function of NCont

If the pull is used instead to compare the two residual distributions from different data sets, the seperation is visible in Figure 18. The width of the pull distribution in $\Xi_c^\pm$ enhanced data is about 0.08 to 0.1 larger compared to the same value in minbias data. In this case, the seperation of these two values gets larger with smaller NCont as expected. The seperation may be visible here, because the PV uncertainty does not account for the slightly larger residual variation induced by the additional $\Xi_c^\pm$ hadron.
Both pull widths are in an acceptable range, and the before mentioned disparities are not large enough to cause a significant difference on the PV position.

3.4.3 Primary Vertex shift

To study the shift of the PV, the shift is calculated by measuring the difference of the distance between the true PV to the true secondary vertex and the distance of the reconstructed PV to the true secondary vertex projected onto the previous vector. The secondary vertex here is referring the decay vertex of a prompt $\Xi_c^\pm$. This makes the shift a one dimensional quantity that does not have to be analised in three different axes. Figure 19 visualises the projection on the x-y-plane.

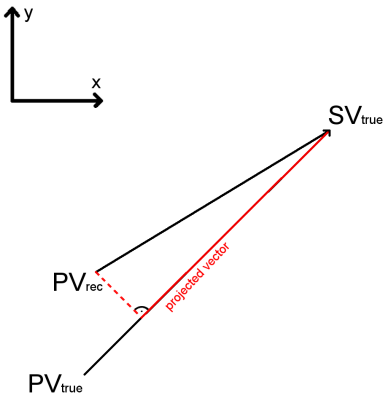

Figure 19: visualised projection of $\overrightarrow{PV_{\text{rec}}SV_{\text{true}}}$ onto $\overrightarrow{PV_{\text{true}}SV_{\text{true}}}$

$$\vec{v}_{\text{projected}} = \frac{1}{|\vec{v}_{\text{t}\to\text{t}}|}\vec{v}_{\text{r}\to\text{t}} \cdot \vec{v}_{\text{t}\to\text{t}} \tag{12}$$

$$d_{\text{difference}} = |\vec{v}_{\text{t}\to\text{t}}| - |\vec{v}_{\text{projected}}| \tag{13}$$

$$\vec{v}_{\text{t}\to\text{t}} : \overrightarrow{PV_{\text{true}}SV_{\text{true}}}$$
$$\vec{v}_{\text{r}\to\text{t}} : \overrightarrow{PV_{\text{rec}}SV_{\text{true}}}$$

Similar to the residual distribution, Equation 12 values can be plotted in a histogram, and fitted with a gaus function to retrieve a mean and width from the distribution. In this case, the distributions are separated into transverse momentum[2] interval to see, if there is any correlation to the shift.

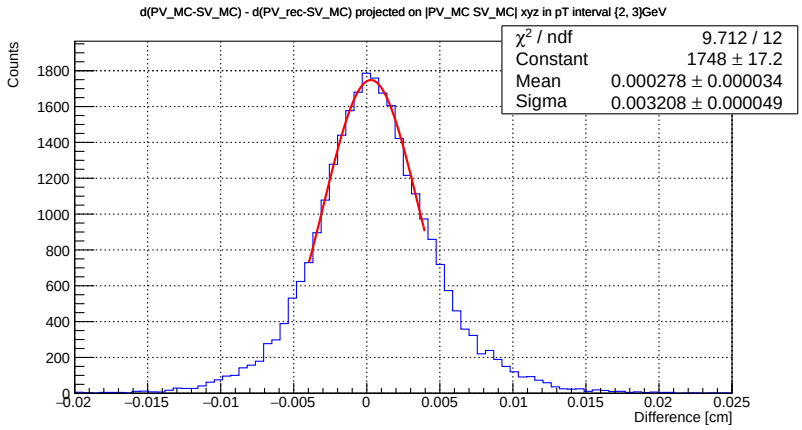

Figure 20: PV shift towards the decay vertex of $\Xi_c^\pm$ according to Equation 13 in the transverse momentum interval of (2 to 3) $\frac{GeV}{c}$. The box states the fit parameters.

According to Equation 13, if the value is positive, the reconstructed PV is shifted towards the true decay vertex of the $\Xi_c^\pm$. The mean of the fit of the distribution in the transverse momentum inteval is $(2.78 \pm 0.34)\mu m$. As argued in the case of the residual distribution, this shift is small compared to the resolution of the detectors, that are used for the track reconstruction. Compared to the average decay length of a prompt $\Xi_c^\pm$ of $137\mu m$, this shift of the mean is only 2%. The width of this distribution is $(32.08 \pm 0.49)\mu m$, which is also smaller compared to the spatial detector resolution, and large enough, that the shift of the mean is not significant.
To reinforce that this distribution depicts the shift of the reconstructed PV towards the secondary vertex, the distribution of the cos (angle) between the two vectors shown in Figure 19, is plotted in a histogram. If this value is one or close to one, the angle between the two vectors is small, and therefore the direction of the two vectors is similar.

[2]this momemtum referrs to the transverse momentum of the $\Xi_c^\pm$

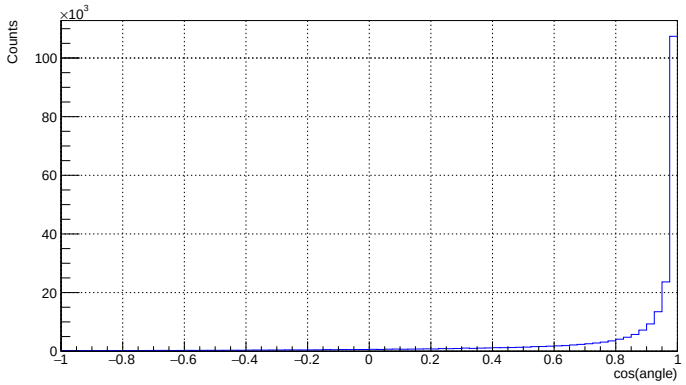

Figure 21: distribution $\cos(angle)$ between the two vectors depicted in Figure 19 in the transverse momentum interval of (2 to 3) $\frac{GeV}{c}$

The distribution of the $\cos(angle)$ has, as expected, a sharp peak at 1, meaning most of the reconstructed PV's are shifted in the direction of the secondary vertex. This histogram together with Figure 20 confirms, that the assumption, the $\Xi_c^{\pm}$ has an influence on the PV, is true. However, as it is the case with the mean of the residual distributions, the shift is not significant.

The KF particle package is able to add the $\Xi_c^{\pm}$ as a track, while removing its daughters to reconstruct the PV. After that, the PV can be refit with the KF method. Then, the same plot as Figure 20 can be made and compared, to figure out, if the $\Xi_c^{\pm}$ or rather its daughter cause the shift.

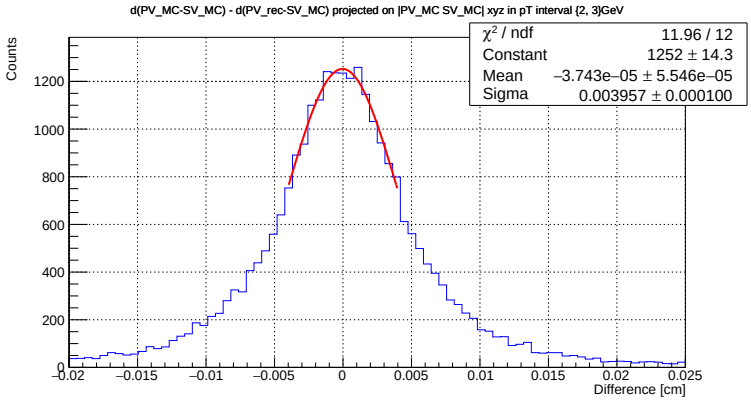

Figure 22: PV shift towards the decay vertex with removed daughter particles of $\Xi_c^{\pm}$ according to Equation 13 in the transverse momentum interval of (2 to 3) $\frac{GeV}{c}$. The box states the fit parameters.

The mean of the fit of this distribution is $(-0.37 \pm 0.55)\mu m$. While the uncertainty on the mean is in the same order as the mean of the distribution in Figure 20, the mean is one order smaller. Now the mean value is together with its uncertainty is within zero, meaning no systematic shift in the direction of the secondary vertex.
Eventhough, the shift shown in Figure 20 is not significant, if the daughter tracks are removed from the PV reconstruction the shift of the mean is gone within uncertainties. This confirms the assumption, that the additional $\Xi_c^{\pm}$ is the cause of the shift in Figure 20 This procedure is easily done in simualted data, since all the parameters from the $\Xi_c^{\pm}$ are known. In real data, the KF package could reconstruct a $\Xi_c^{\pm}$, that does not exist, due to the high combinatorial background in high energy heavy-ion collisions. In this case, it is not feasible to exclude daughter particles from the PV reconstruction, if a short-lived hadron is not reconstructed as such with good certainty.
The earlier distributions show that a single $\Xi_c^{\pm}$ does not shift the reconstructed PV by a significant amount, therefore removing daughter tracks from short-lived particles is not needed with the spatial resolutions of the ALICE Run 2 setup.

4 Results and Conclusion

First in this thesis, the residual of the PV in minbias simulated data is looked at. The distribution shows that with increasing NCont the mean of the residual distributions is systematically shifted in a single direction. The shifts are small compared to the width of the distributions and therefore not significant. The width of these distributions is in the same order as the resolutions of the tracking detectors and therefore acceptable.
The pull distribution of the same data set showed, that the estimated uncertainties of the PV position are good. Hence, the PV in this simulated data set is reconstructed correctly with well-chosen estimated uncertanties and neglible small systematic shifts.

Introducing a $\Xi_c^{\pm}$ hadron into the same data set, results in the PV being shifted towards the decay vertex of this particle, due to the daughter tracks being used in the PV reconstruction. Removing them with the KF particle package, while adding the mother particle into the reconstruction, the previously seen shift of the PV towards the decay vertex is gone. This verifies the claim, that the daughter tracks, decayed from a $\Xi_c^{\pm}$, are the reason behind this shift. The following table shows, how the shift changes in different transverse momentum intervals of the $\Xi_c^{\pm}$.

p_T interval $[\frac{GeV}{c}]$	shift before $[\mu m]$	shift after $[\mu m]$
0 - 2	3.14 ± 0.58	-0.74 ± 0.75
2 - 3	2.78 ± 0.34	-0.37 ± 0.55
3 - 4	3.39 ± 0.27	0.27 ± 0.43
4 - 6	3.10 ± 0.20	0.10 ± 0.29
6 - 8	2.28 ± 0.21	-0.69 ± 0.30

Table 1: mean PV shifts induced by $\Xi_c^{\pm}$ before and after removing the daughter tracks in the reconstruction of the PV position in simulated p-p collision data at $\sqrt{s} = 13TeV$

According to Table 1, there does not seem to be a correlation between the mean shift and the transverse momentum. After removing the daughter tracks from the PV reconstruction, the shift is smaller than its associated uncertainty, except for the last transverse momentum interval. Here, the shift is still within 2.4-σ_{error} to zero and therefore also not significant. The higher uncertainties on the mean can be explained by the different amount of events, that were used for the distributions. The second data set has over all transverse momentum ranges an order of 200 less events compared to the amount of events in minbias data.
All values before and after the removal of daughter tracks in the PV reconstruction, are insignificant compared to the width of the distributions of $30\mu m$ to $40\mu m$. The widths are also well within the resolution of the tracking detectors. Compared to the average decay length of $\Xi_c^{\pm}$ hadrons in high energy collisions, of $137\mu m$, the resolution of the distance between the PV to the decay vertex is good enough to be able to separate those two points of interest, in most events. Though, some $\Xi_c^{\pm}$ can decay so fast, that these two points cannot be distinguished.
The PV vertex is well reconstructed in these simulated data sets. Since the simulation of these data sets is well understood, regarding the position of the PV, the reconstruction of the PV in experimentally measured data can be assumed to be correct aswell within the uncertainties.

5 Outlook

The detector response used in this simulation is modelled after the setup in Run 2 of ALICE. At the time of writing, the ITS of the ALICE detector is already upgraded and in use in Run 3[1]. An upgrade of tracking detectors can improve the track resolution and therefore also the spatial resolution of the PV. If the insignificant shifts are not related to the old ITS detector, a new ITS detector could reach spatial resolutions where the shift in minbias data gets siginificant. The same holds true for the shift induced by $\Xi_c^{\pm}$. Here the better spatial resolution could also result in the PV and decay vertex being seperated that much, that daughter particle tracks are not used in PV reconstruction with the KF particle package in the first place. Also, with higher spatial resolution even faster decaying heavy-flavour hadrons could be analised.

With better resolutions on the PV and decay vertex position, the multiplicity in low transvese momentum ranges of heavy flavour particles, such as the $\Xi_c^{\pm}$ could be determined more accurately, and the understanding of the disparity between simulated and measured baryon-to-meson ratios in low transverse momentum ranges could be improved. This requires that the systematic shifts of the PV do not get significant with increasing track resolution. Also machine learning can help to find heavy-flavour hadrons in low transverse momentum regions, to further improve our understanding of hadronisation. In the case of high energy heavy-ion collisions, it could also help to understand the underlying physics of QGP's and therefore the improve our knowledge of the strong force.

Appendices

Acronyms

ALICE A Large Ion Collider Experiment. 13, 18, 29

ITS Inner Tracking System. 8, 9, 10, 18, 21, 29

KF Kalman Filter. 21, 26, 27, 28, 29

LHC Large Hadron Collider. 3, 8, 10

minbias minimum bias. 13, 14, 22, 23, 24, 28, 29, 32

NCont Number of Contributors. 15, 16, 18, 19, 20, 21, 22, 23, 24, 28, 32

PV Primary Vertex. 6, 7, 8, 13, 14, 15, 16, 18, 19, 20, 21, 22, 24, 25, 26, 27, 28, 29, 32

QCD Quantum Chromo Dynamics. 3, 4

QGP quark-gluon plasma. 3, 4, 29

SDD Silicon Drift Detectors. 9

SM Standard Model. 2, 31

SPD Silicon Pixel Detectors. 9

SSD Silicon Strip Detectors. 9

TOF Time of Flight. 11

TPC Time Projection Chamber. 8, 10, 18

References

[1] B Abelev et al. "Technical Design Report for the Upgrade of the ALICE Inner Tracking System". In: *J. Phys. G* 41 (2014), p. 087002 (cited on page 29).

[2] R.L. Workman et al. *PDG Xi(c)+ data sheet*. 2022 (cited on pages 5, 6).

[3] J. Alme et al. "The ALICE TPC, a large 3-dimensional tracking device with fast readout for ultra-high multiplicity events". In: *Nuclear Instruments and Methods in Physics Research Section A: Accelerators, Spectrometers, Detectors and Associated Equipment* 622.1 (2010), pp. 316–367 (cited on page 19).

[4] Fodor Z. et al. Aoki Y. Endrődi G. "The order of the quantum chromodynamics transition predicted by the standard model of particle physics." In: *Nature* 443 (7112 2006) (cited on page 4).

[5] René Brun et al. *GEANT: Detector Description and Simulation Tool; Oct 1994*. CERN Program Library. Long Writeup W5013. Geneva: CERN, 1993 (cited on page 13).

[6] The ALICE Collaboration et al. "The ALICE experiment at the CERN LHC". In: *Journal of Instrumentation* 3.08 (Aug. 2008), S08002–S08002 (cited on pages 8–10, 19).

[7] Rainer Fries, Vincenzo Greco, and Paul Sorensen. "Coalescence Models for Hadron Formation from Quark-Gluon Plasma". In: *Annual Review of Nuclear and Particle Science* 58.1 (2008), pp. 177–205. eprint: `https://doi.org/10.1146/annurev.nucl.58.110707.171134` (cited on page 4).

[8] Ernst Hellbär. "The ALICE TPC: Optimization of the Performance in Run 2 and Developments for the Future". In: *PoS* LHCP2019 (2019). Ed. by Pablo Roig Garcés et al., p. 240. arXiv: `1909.03746 [physics.ins-det]` (cited on page 10).

[9] Mykhailo Lisovyi, Andrii Verbytskyi, and Oleksandr Zenaiev. "Combined analysis of charm-quark fragmentation-fraction measurements". In: *Eur. Phys. J. C* 76.7 (2016), p. 397. arXiv: `1509.01061 [hep-ex]` (cited on page 4).

[10] Antonin Maire. "Production des baryons multi-étranges au LHC dans les collisions proton-proton avec l'expérience ALICE". Presented 13 Oct 2011. 2011 (cited on page 3).

[11] MissMJ and Cush. *Standard Model of Particle Physics*. 2019 (cited on page 2).

[12] W.-M. Yao et al. Particle Data Group. *PDG charmed baryons*. 2006 (cited on page 5).

[13] "Performance of the ALICE experiment at the CERN LHC". In: *International Journal of Modern Physics A* 29.24 (2014), p. 1430044. eprint: `https://doi.org/10.1142/S0217751X14300440` (cited on page 8).

[14] Carolina Reetz. "Measurement of XicPlus in proton-proton collisions at centre-of-mass energy of 13 TeV with the ALICE detector". Physikalisches Institut, Universität Heidelberg, 2022 (cited on page 6).

[15] I. Kisel S. Gurbonov. "Reconstruction of decayed particles based on the Kalman Filter". In: *CBM-SOFT-note-2007-003* (May 7, 2007) (cited on page 22).

[16] Torbjörn Sjöstrand et al. "An introduction to PYTHIA 8.2". In: *Comput. Phys. Commun.* 191 (2015), pp. 159–177. arXiv: `1410.3012 [hep-ph]` (cited on page 13).

[17] M. Tanabashi et al. "Review of Particle Physics". In: *Phys. Rev. D* 98 (3 Aug. 2018), p. 030001 (cited on page 11).

[18] Jianhui Zhu. "Charm-baryon enhancement and charm fragmentation fractions in small systems measured with ALICE". In: *EPJ Web Conf.* 259 (2022), p. 12003. arXiv: `2108.10938 [nucl-ex]` (cited on page 7).

List of Figures

Additional Figures

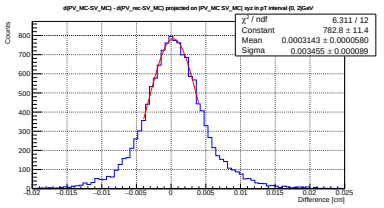

(a) in transverse momentum interval of $(0 \text{ to } 2)\frac{GeV}{c}$

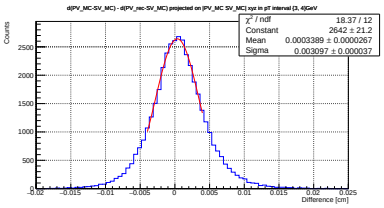

(b) in transverse momentum interval of $(3 \text{ to } 4)\frac{GeV}{c}$

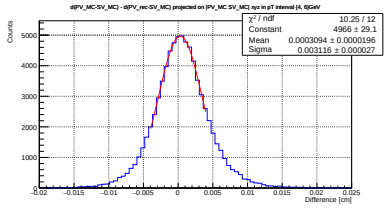

(c) in transverse momentum interval of $(4 \text{ to } 6)\frac{GeV}{c}$

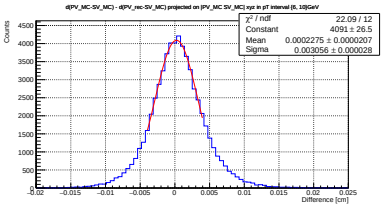

(d) in transverse momentum interval of $(6 \text{ to } 10)\frac{GeV}{c}$

Figure 23: distributions of minbias events according to Equation 13

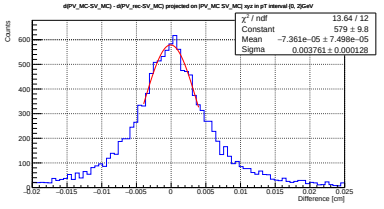

(a) in transverse momentum interval of $(0 \text{ to } 2)\frac{GeV}{c}$

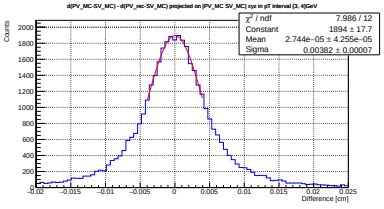

(b) in transverse momentum interval of $(3 \text{ to } 4)\frac{GeV}{c}$

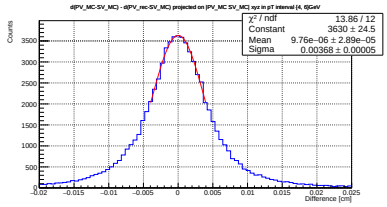

(c) in transverse momentum interval of $(4 \text{ to } 6)\frac{GeV}{c}$

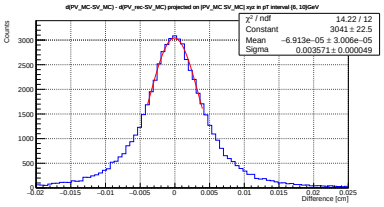

(d) in transverse momentum interval of $(6 \text{ to } 10)\frac{GeV}{c}$

Figure 24: distributions of $\Xi_c^{\pm}$ enhanced events according to Equation 13

Acknowledgement

I want to thank everybody that helped me during writing the thesis and doing analysis. First, I want to thank Silvia Masciocchi for being my Professor and contact for any physics related question, aswell as her great kindness towards everybody, especially with the tight schedule for finishing my bachelor. The same goes for Carolina and Andrea for helping out and sending me sources of different stuff I needed to finish this thesis. I want to thank Bernd, Leon and especially Maurice for always helping out with Latex and Biber, while always encouraging me to finish this thesis.
Also I want to thank my parents for kicking my butt to finally finish this Bachelor.

Thanks to all, who are reading this. This acknowledgement cannot make justice to how thankful I am for having all of you!

Declaration

I declare that the thesis has been composed by myself and that the work has not be submitted for any other degree or professional qualification. I confirm that the work submitted is my own, except where work which has formed part of jointly-authored publications has been included.

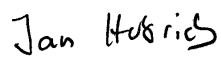

Heidelberg, September 23, 2022

Jan Hubrich